Biosensors and Bioelectronics 133 (2019) 79–85

Contents lists available at ScienceDirect

Biosensors and Bioelectronics

journal homepage: www.elsevier.com/locate/bios

ImmunoSERS microscopy for the detection of smooth muscle cells in atherosclerotic plaques

Ewelina Wiercigroch[a,c], Elzbieta Stepula[b], Lukasz Mateuszuk[c], Yuying Zhang[b], Malgorzata Baranska[a,c], Stefan Chlopicki[c,d], Sebastian Schlücker[b,*], Kamilla Malek[a,c,**]

[a] Faculty of Chemistry, Jagiellonian University, Gronostajowa 2, Krakow 30-387, Poland
[b] Department of Chemistry and Center for Nanointegration Duisburg-Essen (CENIDE), University of Duisburg-Essen, Universitätsstr. 5, 45141 Essen, Germany
[c] Jagiellonian Centre for Experimental Therapeutics (JCET), Jagiellonian University, Bobrzynskiego 14, Krakow 30-348, Poland
[d] Chair of Pharmacology, Jagiellonian University, Medical College, Grzegorzecka 16, 31-531 Krakow, Poland

ARTICLE INFO

Keywords:
ImmunoSERS microscopy
Direct/indirect staining
Atherosclerosis
Smooth muscle cells (SMCs)

ABSTRACT

We investigated the suitability of immuno-SERS (iSERS) microscopy for imaging of smooth muscle cells (SMCs) in atherosclerotic plaques. Localization of SMCs is achieved by using SERS-labelled antibodies direct against alpha-smooth muscle actin (SMA). The staining quality of the false-colour iSERS images obtained by confocal Raman microscopy with point mapping is compared with wide-field immunofluorescence images. Both direct (labelled primary antibody) and indirect iSERS staining (unlabelled primary and labelled secondary antibody) techniques were employed. Direct iSERS staining yields results comparable to indirect IF staining, demonstrating the suitability of iSERS in research on atherosclerosis and paving the way for future multiplexed imaging experiments.

1. Introduction

Atherosclerosis still remains the major cause of cardiovascular events leading to myocardial infarct, heart failure, stroke or sudden cardiac death.(Toth, 2008; Yurdagul et al., 2016) It is a complex and progressive disease characterized by lipid uptake and vascular inflammation and thrombosis in the large and medium-sized arteries (Bennett et al., 2016). One of the important among cellular players in the development of atherosclerotic plaque are smooth muscle cells (SMCs) which are normally present in the tunica media of healthy vessels. Under the influence of fibrogenic mediators and growth factors secreted by T-cells activated in the fatty streak, SMCs change their phenotype from contractile towards synthetic one. Next they proliferate intensively and migrate from the media to the intima (Fig. 1) (Kaperonis et al., 2006; Salvayre et al., 2016). SMCs proliferation plays also predominantly a reparative function since these cells produce extracellular matrix such as elastin, collagen and proteoglycans forming protective layers termed fibrous cap which overlies necrotic core and stabilize the plaque (Bennett et al., 2016; Libby et al., 2011). In turn, apoptotic SMCs promote the atherogenesis process as well as plaque instability. Plaque that is vulnerable – at risk of rupture - have a large necrotic core with lipid-rich foam cells and thin, collagen-poor fibrous cap with few smooth muscle α-actin positive cells derived from vascular SMCs (Bennett et al., 2016; Libby et al., 2011). Stable plaques usually remain clinically silent; therefore, determination of plaque stability is an important clinical issue still presents a great challenge (Salvayre et al., 2016).

Definite identification of unstable plaques as well as understanding the mechanism of its formation still remains a great challenge in medicine and is a crucial step in pharmacological and pre-clinical studies when new therapeutics are tested on animal models (Liang, 2011). Currently, to detect and quantify the composition of atherosclerotic plaques, histological staining (Gajda et al., 2017) or immunohistochemical staining are most frequently employed (Gajda et al., 2008). Immunofluorescence (IF), which is currently the gold standard in visualisation of tissue constituents, relies on the use of antibodies labelled with a fluorescent dye to selectively recognize and localize the target antigen. Mature-differentiated vascular SMCs express selective proteins on their surface, mainly α-smooth muscle actin antigen (SMA) (Bennett et al., 2016; Doran et al., 2008). This antigen is commonly used to localize migration of SMCs from the vessel wall to the atherosclerotic plaque in the artery (Bar et al., 2017; Csányi et al., 2012; Mateuszuk et al., 2016). Two IF methods can be employed, depending on which antibody is conjugated with fluorophore: direct and

* Corresponding author.
** Corresponding author at: Faculty of Chemistry, Jagiellonian University, Gronostajowa 2, Krakow 30-387, Poland.
E-mail addresses: sebastian.schluecker@uni-due.de (S. Schlücker), kamilla.malek@uj.edu.pl (K. Malek).

https://doi.org/10.1016/j.bios.2019.02.068
Received 29 October 2018; Received in revised form 19 February 2019; Accepted 26 February 2019
Available online 11 March 2019
0956-5663/

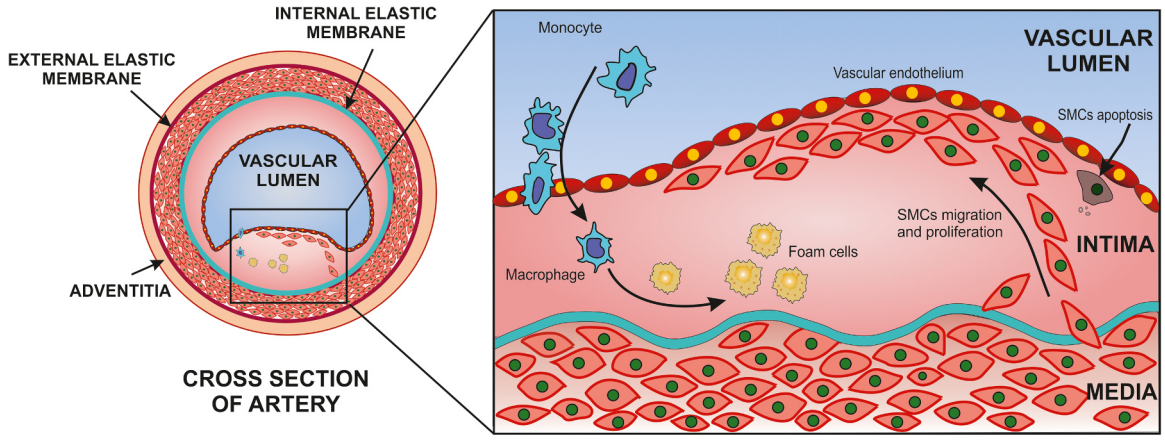

Fig. 1. Schematic representation of the formation of atherosclerotic plaques.

indirect staining (Fig. 2A). In the direct method, the primary antibody conjugated with fluorescent dyes is used to bind the target molecule. This staining protocol is relatively simple and quick but it generally emits a low signal of the tag. In turn, indirect immunochemical staining employs two antibodies: the unlabelled primary antibody to recognize the antigen and the secondary labelled antibody to recognize primary antibodies. The indirect method generates a stronger fluorescence signal and sensitivity than the direct one due to the fact that several secondary antibodies can bind to the primary antibody amplifying the signal, but cross-reactivity of primary and secondary antibodies can be problematic (Taylor and Rudbeck, 2009; Suvarna et al., 2013). Although IF microscopy is commonly used for diagnostics, this technique has certain limitations such as autofluorescence, photobleaching of fluorescent labels or overlapping of absorption/emission bands in multi-target analysis (Woo et al., 2009).

Immuno surface-enhanced Raman scattering microscopy (immunoSERS or iSERS) has been proposed as a new method to detect specific proteins in cells and tissues (Schlücker, 2009; Schlücker et al., 2006). In immunoSERS, fluorophore dye is replaced by a SERS nanotag, i.e., a molecularly functionalized noble metal nanoparticle (Fig. 2B) (Jehn et al., 2009; Wang and Schlücker, 2013). A central advantage of immunoSERS is the multiplexing potential due to the small width of vibrational Raman bands (10–100 times narrower than the broad emission profiles of molecular fluorophores) which reduces spectral overlap (Grubisha et al., 2003). iSERS also overcomes the limitation of photobleaching due to the high photostability of the SERS label/nanotags and minimizes problems with autofluorescence by using red to near infrared laser excitation. The sensitivity of this technique was shown, for example in the detection of prostate specific antigen (PSA) and the tumour suppressor p63 in neoplastic prostate tissues (Jehn et al., 2009; Schlücker et al., 2006; Schütz et al., 2011; Zhang et al., 2017), the human epidermal growth factor receptor 2 (HER2) in breast tissue sections (Wang et al., 2016) and single breast cancer cells (Wang et al., 2017) and BerEP4 antigen in basal cell carcinoma (BCC) of skin (Quynh et al., 2016). iSERS labelled antibody-antigen interactions were also localized in vivo experiments; e.g. Qian and co-workers employed SERS labels conjugated with ScFv antibody to specifically recognize epidermal growth factor receptor (EGFR) on tumour cells surface (Qian et al., 2008)

The present study was undertaken in order to investigate the suitability of iSERS for *ex-vivo* bioimaging of atherosclerosis by comparing its staining quality with IF microscopy as the gold standard. In this work we employed Au nanostars (AuNS) functionalised with α-mercapto-ω-carboxy PEG and 4-nitrothiobenzoic acid (4-NTB) as the Raman reporter and then conjugated to an antibody against α-smooth muscle actin (Fig. 2B). We examined the role of the following two factors: the type of staining (indirect vs. direct) and the type of bioconjugation of the SERS tag to the antibody (with and without the chimeric protein

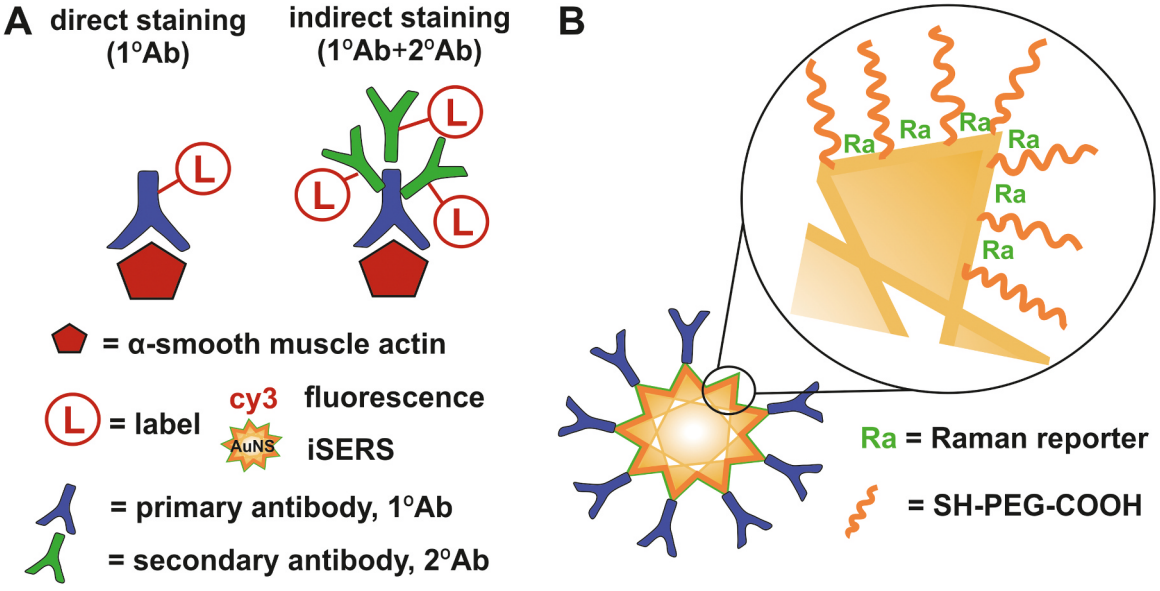

Fig. 2. A. Direct versus indirect immunostaining of α-smooth muscle actin. B. Components of the AuNSs/4-NTB-based antibody-SERS nanotag conjugate.

A/G). The chimeric protein A/G possesses multiple binding sites to the Fc domain of the antibody and supports the antigen recognition sites of the antibody (Salehi et al., 2014). Finally, we compared the performance of iSERS and IF for quantification of SMAs in the plaque.

2. Experimental

2.1. Reagents

Sodium citrate, tetrachloroauric acid ($HAuCl_4{\cdot}3H_2O$), silver nitrate ($AgNO_3$), hydroquinone, 5,5′-dithiobis(2-nitrobenzoic acid) (DTNB), 4-(2-hydroxyethyl) − 1-piperazine ethanesulfonic acid (HEPES), N-hydroxysulfosuccinimidesodium salt (sulfoNHS), 1-ethyl-3-(3-dimethylaminopropyl) carbodiimide (EDC), bovine serum albumine (BSA), paraformaldehyde, paraffin, xylene, ethanol, citrate buffer, normal goat serum (NGS), Hoechst 33258 and glycerol were purchased from Sigma Chemical Co. Phosphate buffered saline (PBS, Gibco™), protein A/G, mouse monoclonal anti α-smooth muscle cell actin (anti-SMA antibody) and secondary goat anti-mouse polyclonal antibody conjugated with fluorophore cyanine3 (Cy3) were received from Thermo Fisher Scientific. Non-fat dry milk powder was purchased from SM Gostyn, Poland. α-mercapto-ω-carboxy PEG (SH-PEG-COOH) was received from Rapp Polymer. Water used throughout all experiments was purified through a Millipore system.

2.2. Instruments

Localization of SERS-labelled antibodies was achieved with a confocal Raman microscope (WITec Alpha 300) equipped with 30 cm focal length, 600 grooves/mm grating spectrometer, and a back-illuminated CCD camera. A 632.8 nm He-Ne laser was employed to excite Raman scattering. The laser was coupled to the spectrometer by an optical fiber with a diameter of 100 μm. Immunofluorescence images were collected using an inverted fluorescence microscope and digital monochromatic camera (Axio Observer D.1 and Axiocam HmR, Carl Zeiss, Germany). Extinction spectra were recorded with the use of a Perkin-Elmer Lambda 950 UV/Vis absorption spectrometer while TEM images were collected using a Zeiss EM 910 instrument. Deparaffinization of tissue sections was carried out using a Leica ST5010 Autostainer XL.

2.3. Synthesis of Au nanostars

Au nanostars (AuNSs) were synthesized by using a seed-mediated method described previously (Schütz et al., 2011). At first, citrate reduction was employed to synthesize 10 nm gold nanoparticle seeds (Turkevich et al., 1951). All solutions were prepared in ultrapure water. A mixture of 900 μL 1% sodium citrate solution, 300 μL 1% $HAuCl_4$ solution and 42.5 μL 0.1% $AgNO_3$ solution was added into 30 mL boiling water. In the next step, 300 μL seeds and 1 mL glycerol were added to 9.8 mL ultrapure water and stirred at 53 *g* for 3 min. The prepared mixture of 22 μL 1% sodium citrate solution, 100 μL 1% $HAuCl_4$ solution and 42.5 μL 0.1% $AgNO_3$ solution was added, followed by the addition of 100 μL 1% hydroquinone solution (after 2 s). Afterwards the colour changed from slightly red to deep blue. After half an hour, Au nanostars were centrifuged for 30 min at 679 *g* and re-dispersed in water. The quality of the Au nanostars was controlled by TEM and UV–vis absorption spectroscopy (Fig. S1).

2.4. Synthesis of SERS-labelled antibodies

1 mL of Au nanostars suspension and 20 μL of 3 kDa 50 μM SH-PEG-COOH solution in MiliQ water were mixed together to incorporate the reactive COOH groups for further bioconjugation to antibodies. The mixture was shaken overnight. Afterwards, functionalized Au nanostars were treated with 10 μL of 4-nitrothiobenzoic acid (4-NTB, 10 mM solution in ethanol) and incubated for 2.5 h. Next, the SERS nanotags were centrifuged and re-dispersed in HEPES buffer (pH = 5.9). For activation of the carboxyl groups, gold nanoparticles were incubated with 10 μL of 6 mM EDC aqueous solution and 10 μL of 15 mM sulfoNHS for 25 min at room temperature (RT). An excess of EDC and sulfoNHS was removed by centrifugation and particles were re-suspended in HEPES buffer. SERS nanotags were optionally incubated with the chimeric protein A/G (2 μg) by 1 h and washed four times in 0.2% BSA/PBS solution. Then, the corresponding primary or secondary antibody (Ab) was added to the functionalised AuNSs suspension (300–500 Ab/AuNS) and left in darkness for 2.5 h at RT. Subsequently, SERS-labelled antibodies were washed four times with 2% BSA/PBS to remove non-conjugated antibodies. Stability of AuNSs and their optical density (OD) were controlled by UV–vis extinction spectra recorded with the use of a spectrophotometer. The final OD of the colloid after bioconjugation to the antibody was adjusted to ca. 1.0.

2.5. Preparation of brachiocephalic artery cross-sections

All experimental procedures involving animals were conducted according to the Guidelines for Animal Care and Treatment of the European Communities and were approved by the Local Ethical Committee on Animal Experiments.

Six-month-old ApoE/LDLR$^{-/-}$ mice with established atherosclerosis (Bar et al., 2017; Csányi et al., 2012; Mateuszuk et al., 2016) were euthanized by intraperitoneal administration of ketamine/xylazine mixture. In anesthetized mice, brachiocephalic arteries (BCA) were dissected out, fixed in 4% buffered paraformaldehyde and embedded in paraffin (FFPE, formalin-fixed paraffin-embedded). Then, 5 μm-thick FFPE cross sections were cut from the artery and mounted on salinized glass slides. Before staining, the sections were automatically deparaffinised in xylene and rehydrated in series of ethanol/water mixture using the autostainer and then rinsed in water. Heat-induced epitope retrieval (HIER) was employed to unmask epitopes altered by fixation. For this purpose, tissue cross-sections were first heated at temperature of 95 °C in citrate buffer (pH = 6) by 60 min, and then cooled down to RT by 20 min. Next, slides were washed with distilled water and PBS solution. Incubation with 5% normal goat serum and 2% non-fat milk in PBS was applied for 0.5 h in RT to increase penetration of antibodies and reduce non-specific binding. Such tissue cross-sections were next stained according to established protocols for IF and iSERS imaging.

2.6. Immunofluorescent (IF) staining

BCA cross-sections were incubated with a primary anti-SMA antibody (mouse monoclonal anti α-smooth muscle cell actin, 1:100 dilution) overnight in humid chambers at RT. Then slides were rinsed with PBS three times to remove unbound antibodies and incubated for 30 min with a 600-fold diluted secondary goat anti-mouse antibody. Following the next wash in PBS, cross-sections were counter-stained with Hoechst 33258 solution specific for DNA (nuclei staining) and again washed with PBS. Afterwards, tissue cross-sections were mounted in 1:1 glycerol:PBS solution to avoid air-drying and immunofluorescence images were recorded. Images were analysed by pixel classification implemented in a Ilastic software (Interactive Learning and Segmentation Toolkit, version 0.5), after training of classifiers separating the object classes. This training was performed in an iterative fashion, where the user gives specific labels, evaluates the interactive prediction and then gives additional labels to correct eventual mistakes. Pictures were divided into separate labels including nuclei, elastic fibers, SMA and background around the tissue cross-section. Before classification, colour and intensity were adjusted to discern objects while a scale for the pixel diameter to calculate biological specimen was σ = 1px. After training, the algorithm constructed the final class assignment in IF images. Calculation of fluorescence signal representing the presence of SMCs was performed using a ImageJ software (version 1.51s, December 2017).

2.7. ImmunoSERS (iSERS) staining

Both direct and indirect iSERS staining in combination with wide-field immunofluorescence (IF) were performed (Zhang et al., 2017). Briefly, direct iSERS staining refers to the use of SERS-labelled primary antibodies and fluorophore-labelled secondary antibodies, while indirect iSERS refers to the use of unlabelled primary antibodies in conjunction with secondary antibodies labelled by both SERS nanotags as well as fluorophores. For the positive direct iSERS staining, cross-sections of the artery were incubated overnight with the SERS-labelled antibody against α-smooth muscle actin. In the case of the indirect method, tissue sections were first incubated overnight with the same primary antibody and after washing in PBS, treated with the SERS-labelled secondary anti-mouse antibody conjugated with Cy3 and with the SERS nanotag. To prepare negative control, 2% BSA/PBS solution was only used and then the tissue was incubated with the secondary SERS-labelled nanotags. All tissue cross-sections were finally mounted in 1:1 glycerol:PBS solution. As for IF, Hoechst staining was optionally performed.

2.8. Collection of Raman microspectroscopic images and their analysis

Localization of SERS-labelled antibodies was achieved by imaging of selected areas of artery cross-sections with the use of a confocal Raman microscope. The laser output power was adjusted in the range of 1.2–2.5 mW. Raman images were collected with a step size of 1 μm under magnification of 20 × (NA = 0.45, an air objective with glass correction) and 40 × (NA = 0.6, an air objective with glass correction). Additionally, Large Area Scan (LAS) was employed to collect Raman images of the whole artery with a step size of 5 μm under a 20x objective. All spectra were recorded with exposure time of 0.15–0.2 s in the region of 0–2600 cm^{-1}.

Initially, SERS images were analysed using a WITec Project Plus software (version 2.10). SERS spectra were pre-processed by a routine cosmic rays removal procedure and baseline correction using autopolynomial of degree 3. Next, cluster analysis (CA) was performed with k-means method (KMC) and the Manhattan distance. The localization of SMAs in BCA tissues was based on the presence of the most intense SERS band at ca. 1340 cm^{-1} in mean spectra which is assigned to the symmetric stretching vibration of the nitro group in 4-NTB. Calculation of pixels assigned to the 4-NTB SERS signal representing the presence of SMAs was performed with the use of a ImageJ software.

3. Results and discussion

We employed conventional IF microscopy with a fluorophore-labelled secondary antibody for confirming the binding specificity of the unlabelled primary antibody directed against α-smooth muscle actin in the BCA tissue after deparaffinization and antigen retrieval according to standard procedures. Fig. 3A shows SMA stained in red together with nuclei stained by Hoechst 33258 in blue. SMCs are distributed in the artery wall as well as on the outer surface and inside of the atherosclerotic plaque. The latter indicates the migration of SMCs due to atherosclerosis. Fig. 3B shows a wide-field fluorescence image when an artery was stained using a SERS-labelled primary antibody followed by the addition of the Cy3-labelled secondary antibody. Both images in Fig. 3A and B show a very good agreement, indicating that tissue deparaffinization, antigen retrieval and labelling of the primary anti-SMA antibody with the SERS nanotag do not affect its binding specificity.

3.1. Direct iSERS staining

The direct immunochemical staining relies on the labelled primary antibody direct against SMA. We used a monoclonal antibody against α-smooth muscle actin conjugated to SERS nanotags in the procedure described above and the commercially available antibody with the fluorophore Cy3 for indirect IF. For a better visualisation of the target of interest in IF images, we used the software “Ilastic” to unambiguously define a class associated with SMCs (Fig. 4A). This segmentation method could distinguish individual constituents as nuclei (blue), elastic fibers (bright green), area of artery occupied by SMA (red) and the remaining part of the blood vessel (dark green). Next, the IF image (Fig. 4B), after segmentation representing only the distribution of the SMA class, was used for the verification whether staining by iSERS imaging is reliable or not (Fig. 4D). For this purpose, LAS (Large Area Scan) implemented in the WITec Raman microscope was employed

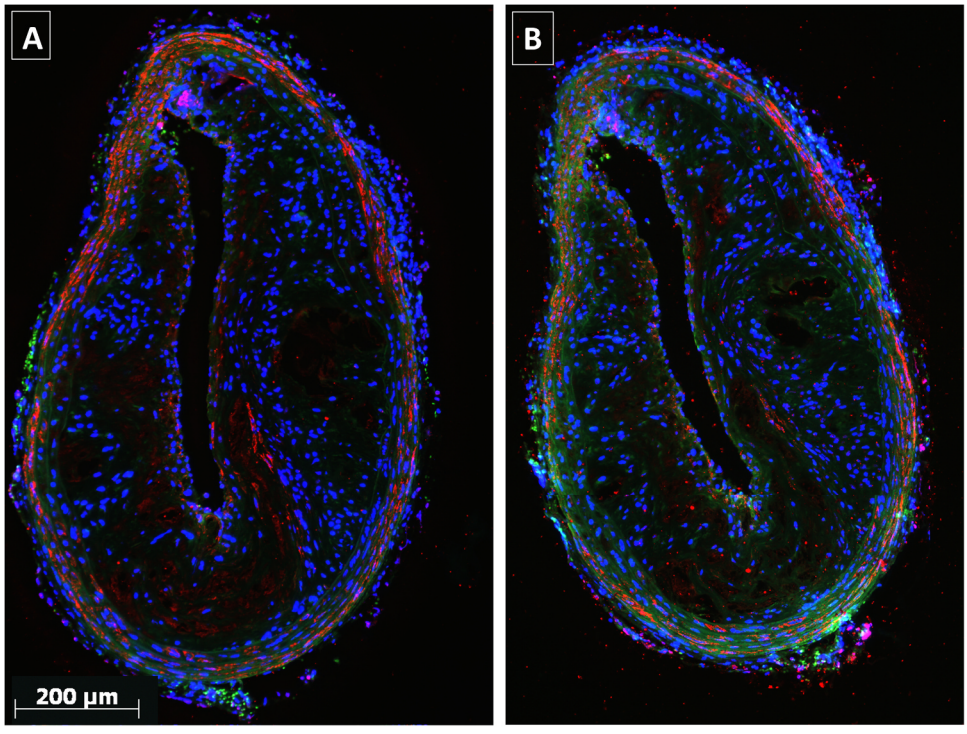

Fig. 3. Immunofluorescence images of two adjacent cross-sections of the ApoE/LDLR$^{-/-}$ arteries obtained by indirect staining: A. Cy3-labelled 2° antibody, unlabelled 1° antibody, B. Cy3-labelled 2° antibody, SERS nanotag-labelled 1° antibody. Red: SMA (Cy3), blue: nuclei (Hoechst 33258), green: autofluorescence of elastin in the aorta wall.

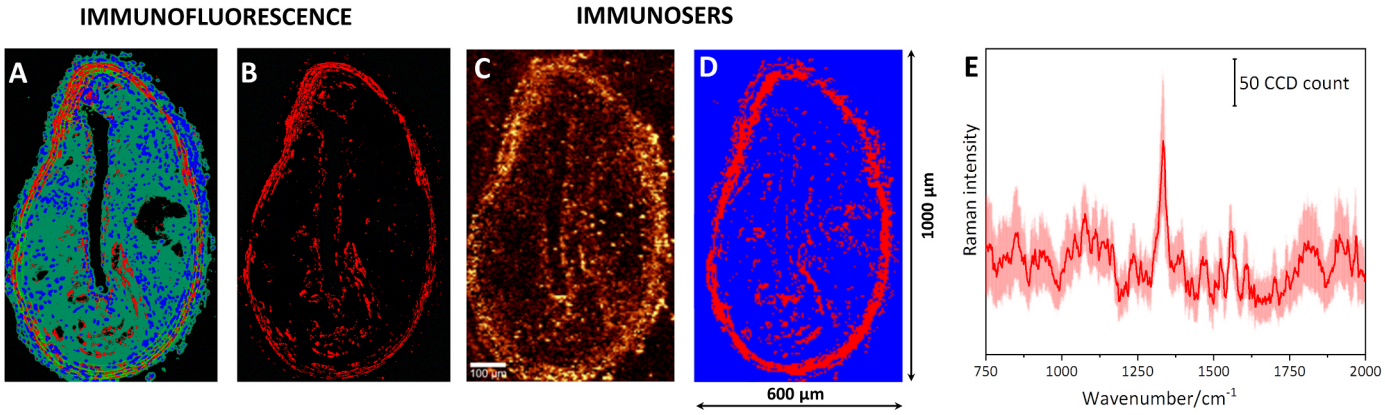

Fig. 4. Detection of SMCs in a BCA cross-section by IF (A, B) and iSERS (C-D) imaging. A. Segmentation of IF image into SMA-positive area (red – Cy3), nuclei (blue - Hoechst), elastic fibers (bright green - autofluorescence) and the remaining part of the blood vessel (dark green). B. IF image of the SMA distribution. C. Univariate false-colour iSERS image (integrated Raman intensity of the marker band at 1340 cm^{-1}). D. Multivariate false-colour iSERS image (k-means cluster analysis) showing the SMCs distribution in the whole aorta (LAS imaging). E. Mean SERS spectrum of the SMA-positive pixels in D with standard deviation (± SD).

with a step size of 5 µm, cf. Fig. 4C-D. On the contrary to high definition Raman microimaging, this technique allows collecting spectra from a large region of interest; in our case it exhibits the presence of SMA in the whole artery (1 mm x 0.6 mm, see Fig. 4), i.e., comparable to the large areas accessible in classic IF. Please keep in mind that the LAS iSERS experiments suffer from spatial undersampling since the employed step size of 5 µm is significantly smaller than the spatial resolution of ca. 0.86 µm. In contrast, the pixel density in the conventional wide-field IF experiments (no scanning of the table) is significantly larger (spatial resolution is ca. 0.5 µm).

Results from a k-means cluster analysis (KMC) performed on the LAS SERS image (Fig. 4D) are very close to those obtained by conventional IF (Fig. 4B). The image contrast in the univariate false-colour SERS image (Fig. 4C) is not as good as for its multivariate counterpart (Fig. 4D), so we suggest that chemometric analysis should be performed for a reliable representation of the antigen distribution. Similar results also have obtained for smaller regions of interest recorded at a smaller step size (Fig. S2). Additionally, it was found that protein A/G coating did not change the efficiency of the detection of SMA (Fig. S4 in SI).

3.2. Indirect iSERS staining with SERS-labelled secondary antibodies

In addition to direct iSERS staining we also performed indirect iSERS staining with an unlabelled primary antibody directed against SMA and a protein A/G-coated SERS nanotag- as well as Cy3-labelled secondary antibody direct against the primary antibody. Using a SERS- and fluorophore-labelled secondary antibody allows us to record both iSERS and IF images. Fig. 5 displays the comparison of classic IF and iSERS images of the two adjacent cross sections of the aorta. A general overview of the distribution of α-smooth muscle actin gathered from the LAS iSERS imaging (Fig. 5C and D) agrees well with the IF images (Fig. 5A and B), confirming a good staining quality in SERS microscopy. Additional high resolution iSERS imaging (small step sizes for large pixel densities) of ROIs 1–2 also precisely detects the presence of SMA in the atherosclerotic plaque and aortic wall (Fig. S3 in SI). Fig. 5E indicates that variation in intensity of the 4-NTB signal is again at the acceptable level and roughly two to three times weaker than found for SERS spectra collected from the direct staining method (Figs. 4E and 5E). Similar to the direct staining method, here protein A/G coating did not change the efficiency of the detection of SMA (Fig. S5 in SI). Overall, both direct and indirect iSERS staining selectively captures the distribution of SMA in the tissue.

3.3. Negative control experiments

Despite the fact that the iSERS-based detection of SMA exhibits the proper distribution of the cells in arteries we carried out negative control experiments without the primary anti-SMA antibody. Arteries

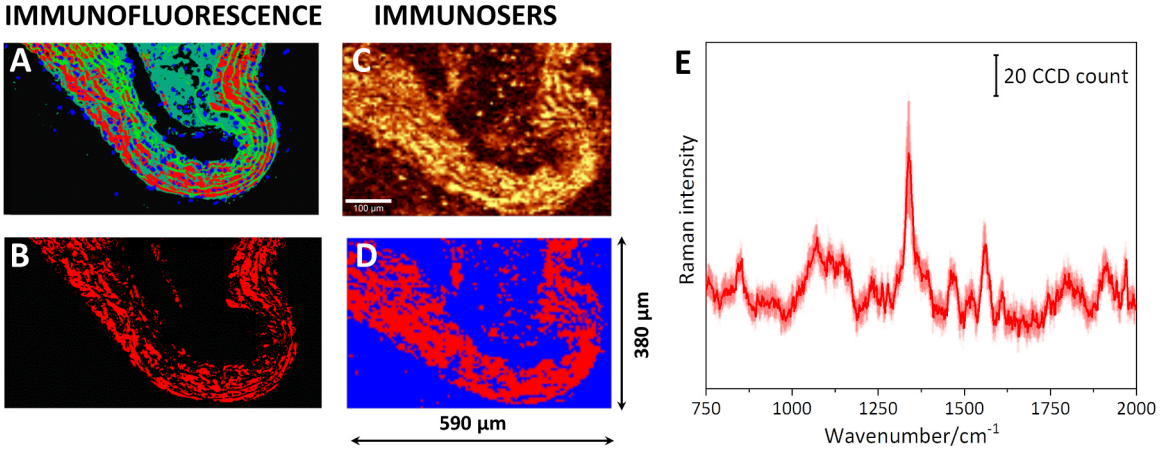

Fig. 5. Detection of SMCs in a BCA cross section by IF and iSERS imaging. For indirect iSERS staining method the secondary goat anti-mouse antibody was labelled by the SERS nanotags coated with protein A/G. A. Segmentation of IF image into SMA-positive area (red – Cy3), nuclei (blue - Hoechst) elastic fibers (bright green - autofluorescence) and the remaining part of tissue including (dark green). B. A false-colour IF image of the SMCs distribution. C. Univariate false-colour iSERS image (integrated Raman intensity of the marker band at 1340 cm^{-1}). D. Multivariate false-colour iSERS (k-means cluster analysis) image showing the SMC distribution in the whole aorta (LAS imaging) E. Mean SERS spectrum extracted from k-means analysis in D with standard deviation (± SD).

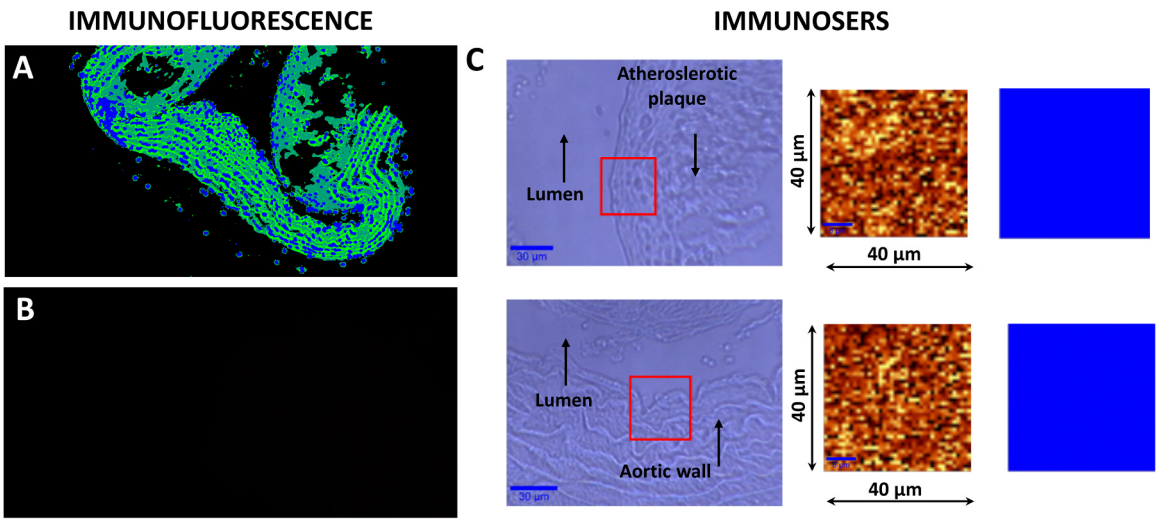

Fig. 6. Negative control experiments without the primary anti-SMA antibody. All other parameters were the same as in Fig. 4. A. Segmentation of IF image into nuclei (blue - Hoechst) and elastic fibers (green - autofluorescence). B. The IF image shows no signal from the Cy3 fluorophore attached to the secondary antibody, i.e., unspecific binding is not observed here. C. selected ROIs in the aortic wall and atherosclerotic plaque (*left*: white light image, *middle*: Univariate false-colour iSERS image, *right*: Multivariate false-colour iSERS image).

were first incubated with 2%BSA/PBS solution and then with conjugates of the SERS nanotags and the secondary Cy3-labelled goat anti-mouse antibody. This antibody does not directly bind to the SMA antigen. Fig. 6 and Fig. S6 show IF images and KMC false-colour maps of iSERS images employing both SERS nanotags with and without protein A/G coating, respectively. No fluorescent signal of Cy3 as well as SERS signal of 4-NTB were recorded, confirming the specificity of conjugates with the antibody against α-smooth muscle actin.

3.4. Quantification of SMAs in the atherosclerotic plaque

An analysis of fluorescence images of biological samples, which are mostly complex and highly content, often requires a segmentation procedure as the first step. Segmentation is a process, in which an image is partitioned into defined regions representing meaningful objects as shown in Figs. 4–6 A. It is a common IF image analysis operation that proceeds quantification of IF signal specific for tissue and cell components.(Dima et al., 2011; Hamilton, 2009) This step is crucial and can strongly affect further analysis and interpretation of image data. However, this procedure is very challenging for the operator since boundaries between objects such as SMCs, nuclei and etc., are difficult to determine and subjective. The commonly employed Ilastic software is considered to be an easy-to-use tool for the segmentation and classification of objects even for the unexperienced user. It is based on interactive machine learning and involves several stages. Firstly, the user needs to set a number of classes and mark a few regions classifying objects of interest. Then, pixel classifiers take into account colour and its intensity, texture, edge as input data. Similar information is also gathered from local pixel neighbourhoods. This phase of the analysis depends primarily on the user choice and consequently has a great impact on the learning procedure (Logan et al., 2016; Sommer et al., 2011). The effectiveness of the Ilastik algorithm is determined by the "out of-baq-error", which is a typical parameter for mathematical operations involving segmentation. Machine learning carries a risk overfitting or underfitting especially when low signal to noise ratio (SNR) of fluorescent images are collected (Hamilton, 2009; James et al., 2007). In this case, IF signal may be indistinguishable from the noise and the precise determination of the location of fluorescently labelled object is distorted. Also photobleaching and overlapping of fluorescence signals makes the identifications of the objects borders of objects difficult. The correctness of the segmentation proven is finally by evaluating the interactive prediction and adding additional labels to examine eventual misclassification (Hamilton, 2009; Sommer et al., 2011). From these reasons an automate segmentation and/or new methods of detection are still needed.

To compare the quantification ability of classic IF and iSERS microscopy, we used the IF image segmented as described above (Fig. 4A) and the iSERS image constructed by k-means cluster analysis (Fig. 4D). To our best knowledge we present this kind of an approach for the first time in the literature. Then, we counted a number of pixels representing SMA in both images by using a Image J program. We calculated in this way that 31% of area α-smooth muscle actin of all detected Cy3 fluorescence signals are located in the plaque of the ApoE/LDLR$^{-/-}$ murine model of atherosclerosis. In turn, the determination of the number of pixels associated with the iSERS-stained α-smooth muscle actin positive area is much easier, as the signal of the Raman reporter in the SERS nanotag conjugated to SMA is easily distinguishable within the tissue cross-section due to the narrow and characteristic band of the reporter. Multivariate analysis like k-means cluster analysis provides a simple classification of the SERS response separating pixels with and without signal in Raman images. In this case, the content of SMA in the plaque of the adjacent cross-section is 28% (Fig. 4D). Taking into account different pixel densities of IF and LAS iSERS images (pixel length 0.5 µm versus 5 µm) and the fact that this is quantification of two adjacent cross sections, the determined small difference between the SMA area in both images shows a potential of iSERS staining as the quantifying imaging methodology. It should be pointed here that autofluorescence can be recorded in pixels neighbouring SERS signal of the Raman reporter and causes sometimes elevated background affecting uni- and multivariate analysis of iSERS images. In such cases the quantitative analysis must be preceded by background correction and/or grouping objects with similar spectral features in cluster analysis. In summary, iSERS microscopy is very well suited for quantification as the narrow Raman peaks can be easily discriminated from background/autofluorescence because of the spectrally resolved detection scheme. This in turn paves the way for a subsequent analysis by powerful multivariate techniques for the classification of pixels.

Immunohistochemical staining is a powerful tool routinely used by pathologists in the diagnostic field, however, features of fluorescent dyes, which exhibit similar excitation wavelength, overlapped broad emission profiles and photobleaching, generate limitations on using this method for simultaneous detection of multiple cell-bound antigens and for their quantification in fluorescence image. iSERS nanotags overcome the problem of photobleaching in IF microscopy and seem to be

highly stable. We also examined the reproducibility of the iSERS signal intensity when data collection is repeated from the same region of the tissue. Fig. S7 in SI displays three false-colour cluster maps. Localization of SMA is correctly determined in the artery wall in each measurement while a number of pixel assigned to 4-NTB varies within 5%. We noted that the signal intensity increased ca. 2-fold after the second laser scanning of the chosen area; very likely local overheating induced by the laser spot causes some deformations in gold nanoparticles shape.

4. Conclusions

Immunofluorescence has a number of limitations in particular for the detection of multiple antigens on the same sample. In this work, we employed immunoSERS (iSERS) microscopy for staining α-actin of smooth muscle cells in the atherosclerosis plaque. Both direct and indirect iSERS staining showed the presence of SMA in the aortic wall as well as within the atherosclerotic plaque area. The iSERS results correspond well to the staining results obtained by IF as the current gold standard. Apparently, the relatively large SERS nanotags did not affect the binding affinity of the primary antibody. This direct staining is preferred as multiple different primary antibodies are available for multiplexing. We propose to analyse the large Raman microspectroscopic data sets by cluster analysis instead of a univariate approach. In this way, one can unambiguously distinguish the SERS signal of the Raman reporter from tissue autofluorescence and/or other spectral artefacts. The employed k-means analysis was also very useful in the quantification of SMA-related pixels.

CRediT authorship contribution statement

Ewelina Wiercigroch: Methodology, Software, Formal analysis, Investigation, Writing - original draft, Visualization. **Elzbieta Stepula:** Methodology, Investigation, Visualization. **Lukasz Mateuszuk:** Methodology, Investigation, Resources. **Yuying Zhang:** Methodology, Investigation. **Malgorzata Baranska:** Conceptualization, Resources, Writing - review & editing, Funding acquisition. **Stefan Chlopicki:** Conceptualization, Resources. **Sebastian Schlücker:** Conceptualization, Resources, Writing - review & editing, Supervision. **Kamilla Malek:** Conceptualization, Resources, Writing - review & editing, Supervision, Project administration, Funding acquisition.

Acknowledgements

This work was supported by the National Centre of Science, Poland (DEC-2013/08/A/ST4/00308 and UMO-2016/21/B/ST4/02151). EW thanks COST Action "Raman-based applications for clinical diagnostics - Raman4Clinics" (BM 1401) for funding her Short-Term Scientific Mission.

Declaration of interests

None.

Appendix A. Supporting information

Supplementary data associated with this article can be found in the online version at doi:10.1016/j.bios.2019.02.068.

References

Bar, A., Olkowicz, M., Tyrankiewicz, U., Kus, E., Jasinski, K., Smolenski, R.T., Skorka, T., Chlopicki, S., 2017. Front. Pharmacol. 8, 1–13.
Bennett, M.R., Sinha, S., Owens, G.K., 2016. Circ. Res. 118, 692–702.
Csányi, G., Gajda, M., Franczyk-Zarow, M., Kostogrys, R., Gwoźdź, P., Mateuszuk, L., Sternak, M., Wojcik, L., Zalewska, T., Walski, M., Chlopicki, S., 2012. Prostaglandins Other Lipid Mediat. 98, 107–115.
Dima, A.A., Elliott, J.T., Filliben, J.J., Halter, M., Peskin, A., Bernal, J., Kociolek, M., Brady, M.C., Tang, H.C., Plant, A.L., 2011. Cytom. Part A 79 A, 545–559.
Doran, A.C., Meller, N., McNamara, C.A., 2008. Arterioscler. Thromb. Vasc. Biol. 28, 812–819.
Gajda, M., Jasztal, A., Banasik, T., Jasek-Gajda, E., Chlopicki, S., 2017. Histochem. Cell Biol. 147, 671–681.
Gajda, M., Jawień, J., Mateuszuk, Ł., Lis, G.J., Radziszewski, A., Chlopicki, S., Litwin, J.A., 2008. Folia Histochem. Cytobiol. 46, 143–146.
Grubisha, D.S., Lipert, R.J., Park, H.Y., Driskell, J., Porter, M.D., 2003. Anal. Chem. 75, 5936–5943.
Hamilton, N., 2009. Traffic 10, 951–961.
James, G., Witen, D., Hastie, T., Tibshirani, R., 2007. An Introduction to Statistical Learning with Applications in R. Springer.
Jehn, C., Kustner, B., Adam, P., Marx, A., Strobel, P., Schmuck, C., Schlucker, S., 2009. Phys. Chem. Chem. Phys. 11, 7499–7504.
Kaperonis, E.A., Liapis, C.D., Kakisis, J.D., Dimitroulis, D., Papavassiliou, V.G., 2006. Eur. J. Vasc. Endovasc. Surg. 31, 386–393.
Liang, M., 2011. Open Cardiovasc. Med. J. 5, 123–129.
Libby, P., Ridker, P.M., Hansson, G.K., 2011. Nature 473, 317–325.
Logan, D.J., Shan, J., Bhatia, S.N., Carpenter, A.E., 2016. Methods 96, 6–11.
Mateuszuk, L., Jasztal, A., Maslak, E., Gasior-Glogowska, M., Baranska, M., Sitek, B., Kostogrys, R., Zakrzewska, A., Kij, A., Walczak, M., Chlopicki, S., 2016. J. Pharmacol. Exp. Ther. 356, 514–524.
Qian, X., Peng, X.H., Ansari, D.O., Yin-Goen, Q., Chen, G.Z., Shin, D.M., Yang, L., Young, A.N., Wang, M.D., Nie, S., 2008. Nat. Biotechnol. 26, 83–90.
Quynh, L.M., Nam, N.H., Kong, K., Nhung, N.T., Notingher, I., Henini, M., Luong, N.H., 2016. J. Electron. Mater. 45, 2563–2568.
Taylor, C.R., Rudbeck, L., 2009. Immunohistochemical Staining Methods Fifth Edition.
Suvarna, K., Layton, C., Bancroft, J., 2013. Bancroft's Theory and Practice of Histological Techniques, 7th ed. Elsevier.
Salehi, M., Schneider, L., Ströbel, P., Marx, A., Packeisen, J., Schlücker, S., 2014. Nanoscale 6, 2361–2367.
Salvayre, R., Negre-Salvayre, A., Camaré, C., 2016. Biochimie 125, 281–296.
Schlücker, S., 2009. ChemPhysChem 10, 1344–1354.
Schlücker, S., Küstner, B., Punge, A., Bonfig, R., Marx, A., Ströbel, P., 2006. J. Raman Spectrosc. 37, 719–721.
Schütz, M., Steinigeweg, D., Salehi, M., Kömpe, K., Schlücker, S., 2011. Chem. Commun. 47, 4216–4218.
Sommer, C., Straehle, C., Kothe, U., Hamprecht, F.A., 2011. Ilastik: Interactive learning and segmentation toolkit. Proc. - Int. Symp. Biomed. Imaging 230–233.
Toth, P.P., 2008. Int. J. Clin. Pract. 62, 1246–1254.
Turkevich, J., Stevenson, P.C., Hillier, J., 1951. Discuss. Faraday Soc. 11, 55–75.
Wang, X.-P., Walkenfort, B., König, M., König, L., Kasimir-Bauer, S., Schlücker, S., 2017. Faraday Discuss. 205, 377–386.
Wang, X.-P., Zhang, Y., König, M., Papadopoulou, E., Walkenfort, B., Kasimir-Bauer, S., Bankfalvi, A., Schlücker, S., 2016. Analyst 141, 5113–5119.
Wang, Y., Schlücker, S., 2013. Analyst 138, 2224–2238.
Woo, M.A., Lee, S.M., Kim, G., Baek, J., Noh, M.S., Kim, J.E., Park, S.J., Minai-Tehrani, A., Park, S.C., Seo, Y.T., Kim, Y.K., Lee, Y.S., Jeong, D.H., Cho, M.H., 2009. Anal. Chem. 81, 1008–1015.
Yurdagul, A., Finney, A.C., Woolard, M.D., Orr, A.W., 2016. Biochem. J. 473, 1281–1295.
Zhang, Y., Wang, X., Perner, S., Bánkfalvi, Á., Schlücker, S., 2017. Anal. Chem. 90, 760–768.